Influence of the Molecular Architecture of Low-Density Polyethylene on the Texture and Mechanical Properties of Blown Films

O. GUICHON, R. SÉGUÉLA, L. DAVID, G. VIGIER

Groupe d'Etudes de Métallurgie Physique et de Physique des Matériaux, UMR CNRS 5510, INSA de Lyon, Batiment Blaise Pascal, 69621 Villeurbanne, France

Received 7 February 2002; revised 30 April 2002; accepted 31 October 2002

ABSTRACT: Three types of low-density polyethylene materials were investigated with respect to the influence of the molecular architecture on the mechanical and use properties of blown films. The materials were a branched polyethylene synthesized by free-radical polymerization under high-pressure (HP-LDPE), a linear ethylene–hexene copolymer (ZN-LLDPE) produced by low-pressure Ziegler–Natta catalysis, and an ethylene–hexene copolymer (M-LLDPE) from metallocene catalysis. The extrusion and blowing conditions were identical for the three materials, with a take-up ratio of 12 and a blow-up ratio of 2.5. The blown films displayed a decreasing puncture resistance in the order M-LLDPE, ZN-LLDPE, and HP-LDPE. In parallel, the tear resistance of the films became increasingly unbalanced in the same order of the polymers. The morphological study showed an increased anisotropy of the films in the same polymer order, the crystalline lamellae being increasingly oriented normal to the take-up direction. This texturing caused a detrimental effect on the mechanical properties of the films, notably increasing the capacity for crack propagation. The phenomenon was ascribed to the kinetics of chain relaxation in the melt that governed the ability of the chains to recover an isotropic state from the flow-induced stretching before crystallization. The puncture resistance was examined in terms of both texture and strain-hardening capabilities.
 J Polym Sci Part B: Polym Phys 41: 327–340, 2003
Keywords: polyethylene (PE); low density; molecular architecture; blown films; puncture; tear; structure; texture; drawing; relaxation time

INTRODUCTION

Since the early 1970s, ethylene/α-olefin copolymers synthesized by Ziegler–Natta catalysis have been largely developed in the domain of blown films for packaging applications, in concurrence with low-density polyethylenes (PEs) produced by high-pressure free-radical polymerization. In recent years, copolymers issued from metallocene technology have taken an increasing place in the field of film blowing because of excellent optical properties combined with remarkable mechanical performances.[1] For the processing difficulties of metallocene copolymers due to narrow molar weight distributions (MWDs), technical solutions have been found by either the incorporation of very low amounts of long side chains or the production of bimodal MWDs.[2,3] There is, however, much work left to do to understand the property upgrade of such novel materials, notably for film applications.

Correspondence to: R. Séguéla (E-mail: roland.seguela@insa-lyon.fr)

Journal of Polymer Science: Part B: Polymer Physics, Vol. 41, 327–340 (2003)

The influence of molecular orientation on the use properties of PE blown films has stimulated profuse studies on the processing–structure and processing–property relationships.[4–31] Nevertheless, little has been accomplished in terms of understanding the influence of the molecular architecture on the structure and mechanical properties of films, via processing conditions. This study focused on three types of low-density PE issued from three different types of polymerization techniques. The differences in the use properties of the blown films were analyzed through the crystalline texture under similar processing conditions for the various polymers.

EXPERIMENTAL

Three low-density PE materials from various sources were studied. The molecular and physical characteristics of the materials are shown in Table 1. M-LLDPE and ZN-LLDPE were linear ethylene–hexene copolymers synthesized by metallocene and Ziegler–Natta catalysts, respectively. The former one, with a narrower MWD, was suspected to contain a few long side chains on the basis of elongational viscosity. HP-LDPE was issued from the high-pressure free-radical polymerization of ethylene in an autoclave. It contained long-chain branches (LCBs) and short-chain branches (SCBs) mainly composed of butyl side groups with minor amounts of ethyl side groups.[32]

Tubular blown films, about 50 μm thick, were processed with an annular die extruder with a 15-cm diameter and a 1.5-mm gap. For the sake of comparison of the blown-film properties, the processing conditions were kept as close as possible for the three materials: flow rate $\approx$ 40 kg/h, melt temperature at the die $\approx$ 190 °C, frost-line height $\approx$ 50 cm, take-up speed $\approx$ 12 m/min, take-up ratio (TUR) $\approx$12 in the so-called machine direction (MD), and blow-up ratio (BUR) $\approx$ 2.5 in the transverse direction (TD). These conditions corresponded to the optimum blowing capabilities of HP-LDPE. The direction perpendicular to the film surface was defined as the normal direction (ND).

For the evaluation of the intrinsic properties of the materials, 1-mm-thick isotropic sheets were also prepared. Pellets were compression-molded for 5 min at 180 °C and subsequently crystallized by being cooled to room temperature (RT) at about 20 °C/min.

The relaxation time, τ, of the materials in the melt was determined from viscoelastic measurements at 190 °C with a Rheometric RSA II apparatus in the cone–plane configuration. The assessment of τ was made from the Cole–Cole diagram of the loss shear modulus versus the storage shear modulus.

Differential scanning calorimetry (DSC) measurements were performed on a PerkinElmer DSC-7 apparatus at a heating rate of 10 °C/min. The calibration of the temperature scale was achieved from the melting scans of high-purity indium and zinc samples at the same heating rate. The melting point (T_f) of the materials was determined at the peak of the melting endotherm of the heating scan following standard cooling from the melt at 10 °C/min.

Small-angle X-ray scattering (SAXS) was used to investigate the crystalline lamellar morphology and texture of the films. The X-ray beam was provided by a Rigaku Cu rotating anode having a 0.1 mm focus and operated at 30 kV and 40 mA. An assembly of two Ni-coated curved mirrors at a right angle was used for a punctual collimation of the incident beam. The scattered intensity was detected with a position-sensitive linear counter selecting Cu Kα X-ray photons. It was located at 80 cm of the sample, with a vacuum section between the detector and sample. For optimum X-ray absorption, approximately 2-mm-thick samples were made by several pieces of films or compression-molded sheets being piled up. For blown films, the through-view scattering curves were

Table 1. Molecular and Physical Characteristics of the Materials

Polymer	MFI (g/10 min)	M_n (kDa)	M_w (kDa)	Density (g/cm^3)	τ (s)
HP-LDPE	0.8	17	170	0.924	2.70
ZN-LLDPE	1.0	28	116	0.918	0.05
M-LLDPE	1.0	42	108	0.920	0.02

recorded parallel to both MD and TD. Edge-view scattering curves were also recorded parallel to MD and ND. For a comparison of the scattering intensity profiles versus the scattering vector of the various materials, all the intensity data in arbitrary units were corrected for the background scattering, absorption, and Lorentz factor.[33] The transmission coefficient for every sample was determined from the ratio of the peak intensities of the incident beam with and without the sample. The intercrystalline long period, L, was directly determined from the correlation peak of the intensity profile. The average crystal thickness, L_c, was assessed from the equation $L_c = L\phi_c$, which assumes much greater length and width of the crystalline lamellae than their thickness. The crystal volume fraction, ϕ_c, was computed from the density, ρ, of the material with the relation $\phi_c = (\rho - \rho_a)/(\rho_c - \rho_a)$, where $\rho_c = 1.000$ g/cm^3 and $\rho_a = 0.855$ g/cm are the densities of perfectly crystalline orthorhombic PE and amorphous PE, respectively.[34]

Wide-angle X-ray scattering (WAXS) experiments were performed in the transmission mode with monochromatic Cu Kα radiation. Through-view patterns on films were recorded on a two-dimensional CCD camera.

K The tear and puncture resistance of the blown films were determined at RT according to the standard Elmendorf test (ASTM D 1922) and dart impact test (ASTM D 1709), respectively. Conventional tensile stress–strain measurements were carried out at RT on an Instron testing machine at a crosshead speed of 100 mm/min, with dumbbell samples 100 mm in gauge length. Both isotropic sheets and films were tested. For films, tensile experiments were carried out along MD and TD. The reported curves are representative of three different measurements.

Shrinkage measurements of the blown films above T_f were carried out with 5 cm × 5 cm specimens suspended by small clamps into an oven at 130 °C for 5 min. Shrinkage data along MD and TD were assessed from the ratio of the dimension change to the initial dimension of the film piece. Experiments at various temperatures between 125 and 135 °C showed some temperature dependence of the M-LLDPE shrinkage, whereas ZN-LLDPE and HP-LDPE proved to be almost insensitive. However, the ranking of the materials in terms of shrinkage capacity did not depend on temperature.

TEAR AND PUNCTURE RESISTANCE OF THE FILMS

M An examination of the dart impact data of films in Table 2 shows that HP-LDPE has the lowest puncture resistance of the three materials. Moreover, the perforation of HP-LDPE films appears as an elongated crack parallel to TD. In contrast, ZN-LLDPE exhibits an elongated perforation parallel to MD. M-LLDPE displays the best film puncture resistance, and the perforation is fairly circular. These observations are relevant to the structural anisotropy of both HP-LDPE and ZN-LLDPE, whereas M-LLDPE looks rather isotropic.

Under tear testing, HP-LDPE displays the lowest capabilities of the three materials. It is notably unbalanced, with a higher tear resistance in MD. The better tear performances of M-LLDPE are fairly well equilibrated along MD and TD. M-LLDPE is challenged by ZN-LLDPE with respect to the level of tear resistance, even though the latter displays nonequilibrated properties, the higher tear resistance being in TD.

In summary, the puncture and tear properties of M-LLDPE are fairly high and isotropic despite the largely unbalanced TUR and BUR of the films. In contrast, HP-LDPE and ZN-LLDPE reveal strong anisotropy along TD and MD that suggests chain orientation and/or crystalline texturing of the films. The anisotropy effect is, however, opposite in the two materials, despite identical blowing conditions: ZN-LLDPE is more tear-resistant in TD than in MD, whereas HP-LDPE displays greater tear resistance in MD. Similar observations of opposite behavior between linear PE films[11,15,23,24,30] and branched PE films[20,28] can be found in the literature for usual blowing conditions notably involving TUR > BUR. This surprising finding suggests that the intuitive picture of an improved tear resistance normal to the

L

Table 2. Puncture and Tear Properties of the Films

Film	Puncture Resistance (load in g)	Tear Resistance (Force in cN)	
		MD	TD
HP-LDPE	135 ± 20	123 ± 12	81 ± 4
ZN-LLDPE	345 ± 25	212 ± 12	295 ± 12
M-LLDPE	1250 ± 80	181 ± 5	198 ± 5

main-chain orientation of the films, which is MD in most cases, does work for ZN-LLDPE but does not work for HP-LDPE. Otherwise, it was proposed by Kim and coworkers[23,24] and Andre et al.[29] that crystalline lamellar orientation might be more important than the molecular orientation with respect to tear resistance because lamellae are likely to act as obstacles to crack propagation. This is the reason for the following structural study.

STRUCTURE AND TEXTURE

Compression-Molded Sheets

For the three kinds of PE studied, the SAXS data of Table 3 reveal very similar if not equal crystal thicknesses for isotropic sheets and films. This is relevant to the relatively low sensitivity of low-density PE materials to the cooling rate, that is, about 20°/s for blown films and 20°/min for compression-molded sheets.

Considering the densities of the materials under investigation and using the data from Kuhn and Krömer,[32] we can assume a butyl SCB rate of about 17/1000 C (where C is a carbon atom of the polymer backbone) for HP-LDPE, whereas a rough figure of 18/1000 C can be assumed for the butyl SCB concentration of both ZN-LLDPE and M-LLDPE according to various literature data.[23,35,36] Under such considerations, it turns out that the average distance between short branches along the main chain is about 7 nm. The quite good consistency of this figure with the crystal thickness of the materials reported in Table 3 supports the largely accepted scheme of an exclusion from the crystalline phase of the SCB having two carbon atoms or more. As a matter of fact, if the SCB bulkiness prevents the counit inclusion in the crystal lattice due to crystal growth, one should expect L_c to be governed by the average length of the crystallizable methylene sequences.[37]

M-LLDPE and HP-LDPE have somewhat lower L_c values (Table 3) than ZN-LLDPE, with a concomitant lower T_f. This is relevant to the more uniform distribution of the counits or SCBs of the former two materials. Heterogeneous ZN copolymers are indeed well known to grow thicker crystals with higher T_f values than homogeneous copolymers or branched PEs of similar crystallinity[38–40] because of almost counit-free chains. This is an advantage for some applications such as hot tack but is prejudicial for optical properties, for instance.[38] This structural difference should nonetheless have very little impact on tear and puncture properties, notably on anisotropy.

Blown Films

Figure 1 shows the through-view SAXS profiles from the films of the three materials recorded parallel to MD and TD. The nearly identical intensity profiles of Figure 1(c) indicate a fairly isotropic structure for M-LLDPE in the plane of the film, which contrasts with the strong anisotropy of the HP-LDPE film revealed in Figure 1(a). Not only is the SAXS correlation peak much higher along MD than along TD for HP-LDPE, but the peak intensities are respectively greater and smaller than those of the M-LLDPE SAXS peak. This anisotropy of HP-LDPE is relevant to the well-known flow-induced row texture of blown films and spun fibers[41] with the crystalline lamellae essentially normal to MD. The ZN-LLDPE film displays an intermediate state of orientation [Fig. 1(b)] between HP-LDPE and M-LLDPE films [Fig. 1(a,c)], the crystalline lamellae being still preferentially normal to MD.

SAXS measurements from the edges of the films corroborate the row texture of the HP-LDPE

Table 3. Thermal and Structural Characteristics of the Films and Isotropic Sheets

	T_f (°C)			L (nm)		L_c (nm)	
Polymer	Film	Sheet	ϕ_c[a]	Film	Sheet	Film	Sheet
HP-LDPE	110	108	0.47	12.5	12.5	5.9	5.9
ZN-LLDPE	124	127	0.43	16.0	17.0	6.9	7.3
M-LLDPE	116	120	0.45	14.0	14.0	6.3	6.3

[a] Computed from the nominal densities of the materials listed in Table 1.

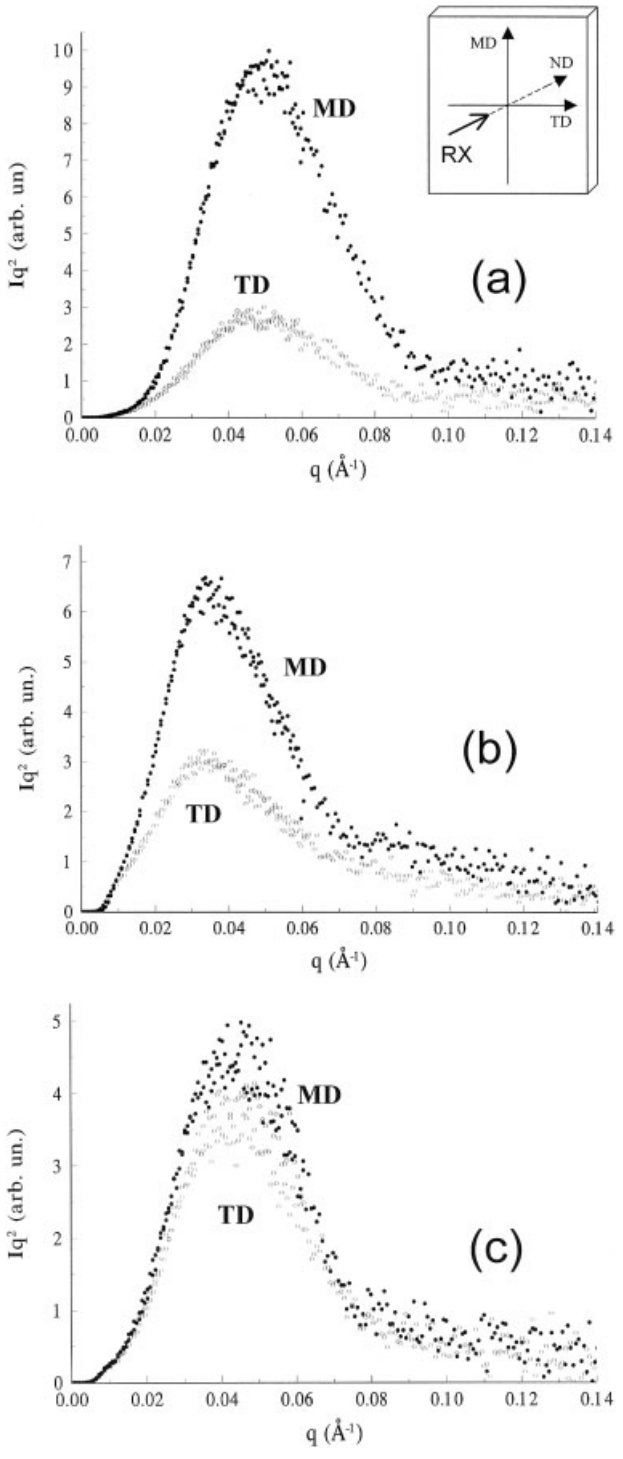

Figure 1. Through-view SAXS intensity profiles of the blown films recorded parallel to MD and TD: (a) HP-LDPE, (b) ZN-LLDPE, and (c) M-LLDPE.

film, as judged from Figure 2. As a matter of fact, the edge-view profile recorded along MD shows a much stronger intensity maximum than the one along ND. This is clear evidence that most of the crystalline lamellae lie normal to MD. It is quite surprising that M-LLDPE also displays some anisotropy from the edge view of the film [Fig. 2(b)], which suggests that the elongated crystalline lamellae, otherwise lamellar ribbons, have a predominant orientation along ND. Considering the through-view isotropy of M-LLDPE [Fig. 1(c)], we may ascribe this finding to a preferred orientation of the growth direction of the lamellar ribbons, namely, the crystallographic *b* axis,[42] along the temperature gradient[43,44] during the crystallization step, that is, the film thickness in this instance. This effect should also exist for HP-LDPE but is certainly hidden by the flow-induced row texture. The M-LLDPE film may, therefore, be called orthotropic rather than isotropic.

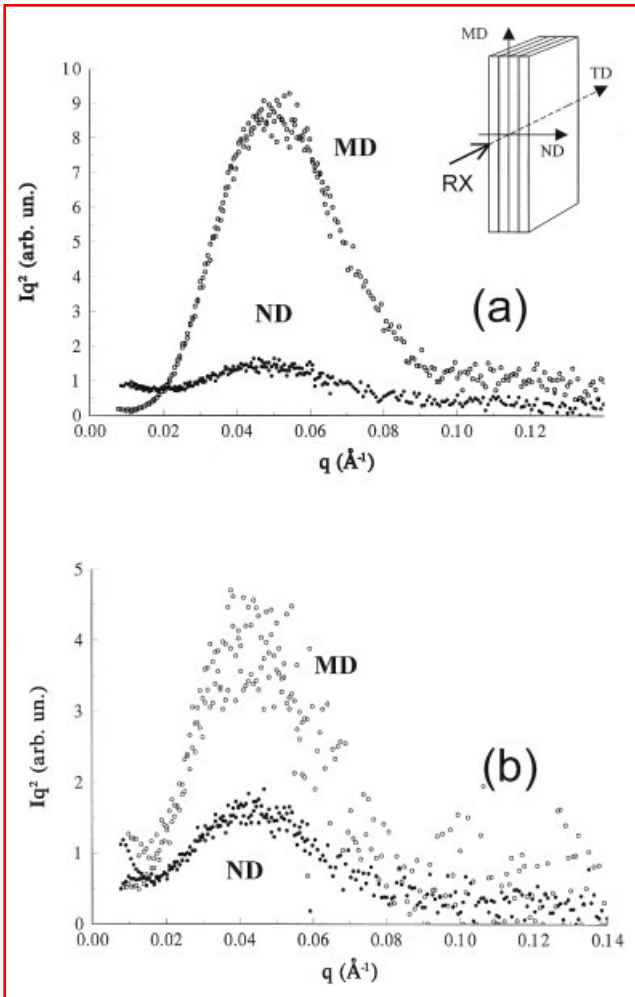

Figure 2. Edge-view SAXS intensity profiles of the blown films recorded parallel to MD and ND: (a) HP-LDPE and (b) M-LLDPE.

The WAXS patterns of Figure 3 show a reinforcement of the inner (110) and outer (200) reflections in the MD and TD positions, respectively, for HP-LDPE and ZN-LLDPE films. This is relevant to the so-called low-stress row structure of Keller and Machin,[41] which corresponds to a preferred orientation of the twisted crystalline lamellae with the crystallographic *b* axis, that is, the growth axis, roughly parallel to TD, and the *a* and *c* axes being randomly distributed about TD because of the lamellar twisting. The diagonal reinforcement of the (110) reflection for the HP-LDPE film [Fig. 3(a)] reveals a sharper orientation of the *b* axis parallel to TD than for ZN-LLDPE. The M-LLDPE film displays no preferred orientation of the crystalline phase in the film, indicating isotropy or orthotropy. These WAXS data corroborate the conclusions from SAXS.

With respect to the compression-molded sheets, the unreported WAXS patterns confirm the completely isotropic structure for the three materials.

UNIAXIAL TENSILE DRAWING

Compression-Molded Sheets

In conjunction with structural investigations, several authors have used uniaxial tensile drawing of blown films to understand the tear and puncture behavior.[10,20,24,30,31] Because the dart test is equivalent to a multiaxial tensile test, it is obvious that uniaxial testing at various orientations with respect to MD may be valuable for understanding the puncture resistance of films. In contrast, tensile drawing does not seem to have significant relevance to tear resistance, at first sight. Nevertheless, it clearly appears from the literature data[24,30] that the more unbalanced the tear resistance is in MD and TD of blown films, the greater the departure is of both the strain hardening and the elongation at break of the films upon tensile drawing along MD and TD.

The engineering stress–strain curves of the isotropic compression-molded polymers are reported in Figure 4. The three materials have about the same yield stress at 10 ± 1 MPa. However, HP-LDPE displays a lower elongation at rupture and a lower strain hardening than ZN-LLDPE. This well-known phenomenon can be ascribed to the bulkiness of the branched molecules with LCBs, which limit chain overlapping in the melt. A re-

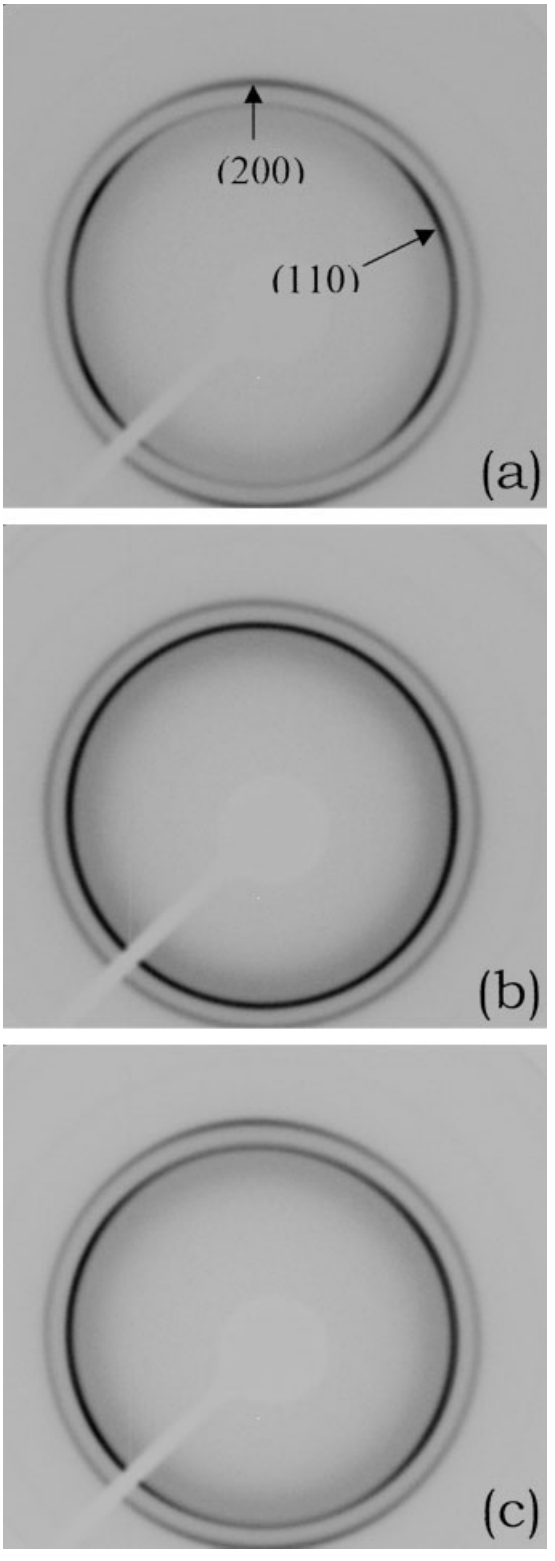

Figure 3. Through-view WAXS patterns of the blown films: (a) HP-LDPE, (b) ZN-LLDPE, and (c) M-LLDPE (MD is vertical).

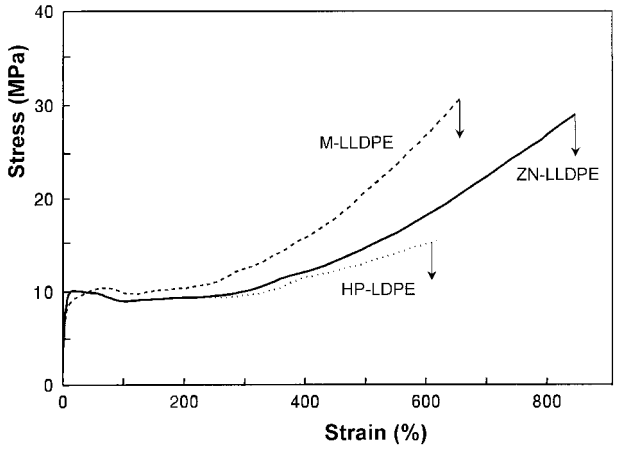

Figure 4. Engineering stress–strain curves at RT of compression-molded sheets from the HP-LDPE, ZN-LLDPE, and M-LLDPE materials.

sult of this phenomenon is to reduce the entanglement density and the intercrystalline tie chain frequency in the crystallized material.[38] This point is more specifically addressed in the Discussion section.

M-LLDPE displays a lower elongation at break than ZN-LLDPE but exhibits a surprisingly higher strain hardening. A similar observation in a previous study[40] has been ascribed to a higher concentration of entanglements and tie chains in M-LLDPE because of the homogeneous distributions of the counits, which not only reduces crystal thickness in comparison with ZN-LLDPE (see the previous section) but also reduces the processes of regular folding and reeling-induced disentanglement of the chains during crystallization. Therefore, in contrast to HP-LDPE, which is less resistant to tensile drawing than ZN-LLDPE because of lower overlapping of the chains, M-LLDPE looks significantly more resistant than ZN-LLDPE because of better chain intertwining.

Blown Films

Figure 5 shows the tensile stress–strain curves along MD and TD for the three types of films. M-LLDPE displays quite similar behavior when tested along MD and TD [Fig. 5(c)]. Besides, the stress–strain curves resemble that of the isotropic compression-molded sheet (Fig. 4), notably with respect to extension at break and strain hardening. This finding means that M-LLDPE is almost isotropic and accounts for the well-equilibrated TD and MD tear resistance. In contrast, HP-LDPE and ZN-LLDPE films exhibit unbalanced tensile properties along MD and TD [Fig. 5(a,b)],

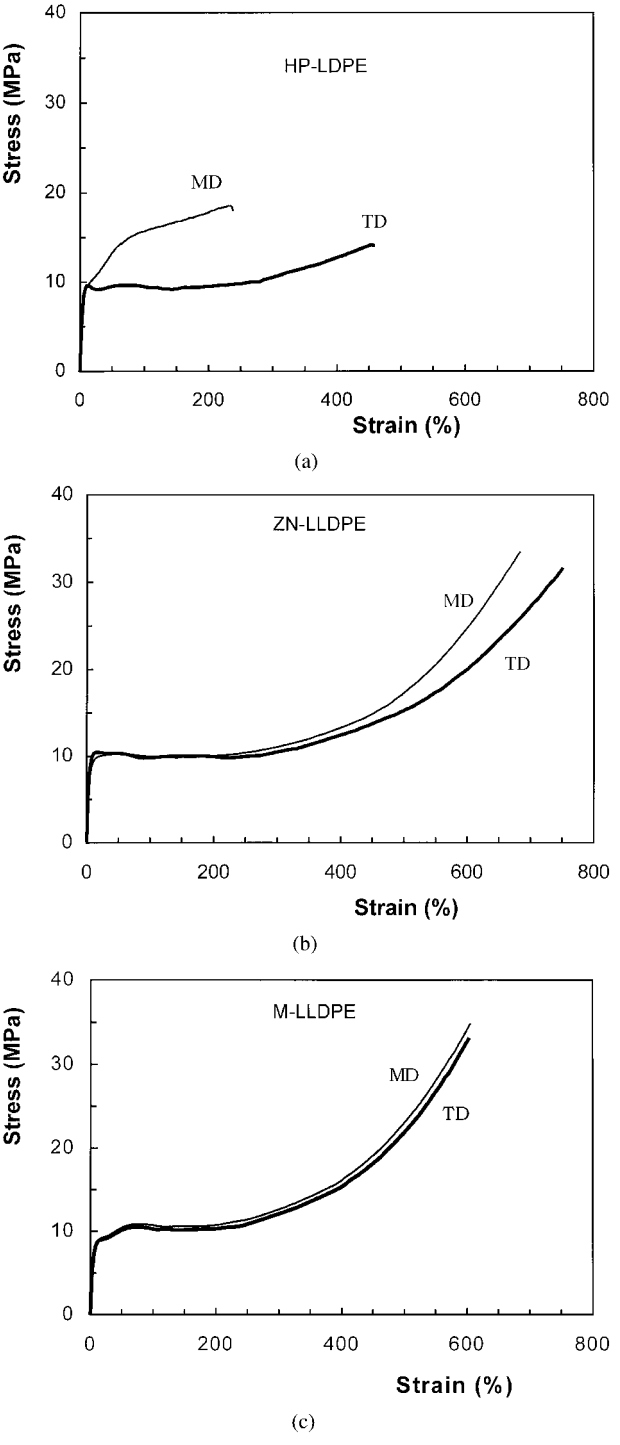

Figure 5. Engineering stress–strain curves at RT of the blown films along MD and TD: (a) HP-LDPE, (b) ZN-LLDPE, and (c) M-LLDPE.

notably a lower drawability along MD. Besides, drawability in both directions is lower than that of the compression-molded sheets, this phenomenon being much more pronounced for HP-LDPE. This means that both ZN-LLDPE and HP-LDPE display a higher degree of chain extension in MD. In parallel to its much reduced drawability in MD, HP-LDPE displays a surprising jump of the yield stress to about 15 MPa in MD, in contrast to 10 MPa in TD and for the isotropic sheet. This point is specifically addressed in the Discussion section.

The nearly isotropic properties of the M-LLDPE film suggest that the chains have an almost undisturbed coil conformation despite the largely unbalanced TUR and BUR. In contrast, the unbalanced properties of ZN-LLDPE and HP-LDPE films, together with the significant loss of drawability with respect to their isotropic compression-molded counterparts, are relevant to a significant chain extension in the films. This is evidence that the flow-induced extension of the chains during the blowing process has been partly frozen-in during the solidification step, for both HP-LDPE and ZN-LLDPE. This suggests that these two materials have less capacity for chain relaxation in the melt than M-LLDPE, HP-LDPE being the most quenching-sensitive.

The strain hardening of M-LLDPE, both in films and sheets, is somewhat higher than that of the two other materials. Such a property notably reduces the capacity for plastic instabilities during deformation and, therefore, contributes to the improvement of the puncture resistance of the M-LLDPE film. As a corollary to its higher strain hardening, the M-LLDPE film exhibits lower standard deviations of the tear and puncture resistance data (Table 2) that are relevant to a weaker sensitivity to structural film defects such as thickness fluctuations and inclusions.

DISCUSSION

Table 4 reports a summary of the film properties. Both structural and mechanical anisotropy increase in the order M-LLDPE, ZN-LLDPE, and HP-LDPE. In comparison with the compression-molded sheets, the tensile drawing of the films clearly reveals that, despite the similar blowing conditions, the three materials have different levels of chain extension (otherwise chain unfolding) depending on the chain architecture. The shrinkage data of Table 4, which reflect the degree of chain extension frozen in the films, thoroughly support this conclusion. The material rankings for the degree of chain extension of the films are the same as the previous ones for the increasing anisotropy. The different levels of chain extension of the three materials, superimposed on the crystalline texturing, can be analyzed with regard to the rheological properties of the materials, in relation to the processing conditions.

Chain Relaxation during Blowing

The mean relaxation time data of Table 1 show that the three materials have quite different capabilities of relaxation in the melt of the flow-induced chain extension accompanying TUR $\approx$ 12 and BUR $\approx$ 2.5. Considering the frost-line height of about 50 cm and the take-up speed of 12 m/min used in the blowing process, one may estimate that the molten material experiences an extensional flow for about 2.5 s before solidification. The actual duration of the extensional flow is certainly shorter than this figure because the chain-extension pathway along TD and MD is not uniform over the whole length between the die and the frost line. Therefore, it is clear that the relaxation time of HP-LDPE may hardly allow a

Table 4. Summary of the Data on the Texture, Mechanical Properties, and Use Properties of the Blown Films

Polymer	Texture	Elongation at Break	Dart Impact	Tear Resistance	Thermal Shrinkage
HP-LDPE	Highly anisotropic lamellae/(TD)	TD $\gg$ MD	Rather low	Low and unbalanced (MD > TD)	70% MD 10% TD
ZN-LLDPE	Anisotropic lamellae/(TD)	TD > MD	Good	High and unbalanced (MD < TD)	40% MD 5% TD
M-LLDPE	Isotropic	TD $\approx$ MD	High	High and balanced	10% MD 0% TD

recovery of the flow-induced chain extension during the time that elapses between extrusion and crystallization. In contrast, ZN-LLDPE and M-LLDPE are clearly capable of relaxing the flow-induced chain extension, at least in part, before crystallization.

Ghaneh-Fard et al.[45] pointed out the role of chain relaxation on the orientational behavior of blown films in the melt before crystallization. Yu and Wilkes[22] emphasized the drastic effect of long chains having a long relaxation time on film orientation. Lu et al.[30,31] demonstrated that the shape of the incipient bubble, which is governed by the cooling conditions, strongly influences the film texture and properties because of the modifications of the relaxation capabilities of the molten material along MD and TD. Prasad et al.[46] also reported recently that LCBs in linear HDPE induce a strong texturing of blown films because of a drastic increase of the longest relaxation time in the melt. In contrast, Plumbey et al.[20] reported a nearly isotropic structure for metallocene copolymer films, despite unbalanced TUR and BUR values. Recently, Legros et al.[26] reported that metallocene copolymers afford significantly less oriented films than corresponding Ziegler–Natta copolymers. These observations, which corroborate our own findings on the M-LLDPE film, can unambiguously be ascribed to the rather short relaxation time of metallocene copolymers, which is due to the narrow MWD.

With respect to the shrinkage behavior, the data reported in the last column of Table 4 show that the three kinds of films systematically shrink more along MD than along TD. However, these data also display quite different shrinkage capabilities of the films in the order HP-LDPE > ZN-LLDPE > M-LLDPE. The very low shrinkage of the M-LLDPE film is notably indicative of a very faint chain extension. This finding thoroughly agrees with the MD and TD tensile drawing behavior of the M-LLDPE film, which closely resembles that of the compression-molded sheet. Therefore, the so-called orthotropy of the M-LLDPE film, which has been concluded from the standpoint of texture, turns out to be very close to isotropy from a mechanical standpoint.

ZN-LLDPE is slightly unbalanced with respect to the stress–strain curves in TD and MD [Fig. 5(b)], and the curves are not so far from the one of the isotropic sheet (Fig. 4). In contrast, HP-LDPE is highly unbalanced, and the stress–strain curves reveal higher drawability along TD. Besides, HP-LDPE displays significantly lower strain hardening and lower stress at break than ZN-LLDPE and M-LLDPE. The strong mechanical anisotropy and poor performances at rupture provide an explanation for the relatively poor dart impact resistance of the HP-LDPE film.

The contrasting behaviors of HP-LDPE and ZN-LLDPE with respect to tearing, that is, the higher tear resistance being along MD and TD, respectively, suggest a competition between crystal orientation and chain extension in the process of crack propagation, which is discussed later.

The quite different degrees of texturing of the three kinds of materials, which greatly influence their tensile drawing behavior and use properties, can be explained by the rheology of the materials: the much shorter relaxation time of M-LLDPE in the melt allows an almost complete relaxation of the flow-extended chains toward the stable random coil conformation, during the time elapsing between the die and the frost line. ZN-LLDPE and HP-LDPE are only partly able to relax the chain extension before crystallization, the latter having greater hindrance for chain relaxation.

Chain Intertwining

The entanglement of chains has a tremendous effect on both rheological and solid state properties. It strongly contributes to the strain-hardening effect in the elongational viscosity, which is a basic factor of bubble stability during tubular film blowing.[47] It is also a determining factor for the mechanical properties of blown films via drawability and strain hardening. However, it is noteworthy that branched and linear PEs display a puzzling opposite behavior with respect to this latter property: namely, the strain hardening of melt elongational viscosity is high for branched PEs and low for linear PEs,[47] whereas just the opposite trend is observed for the solid materials.[38]

This phenomenon emphasizes the drastic influence of molecular dynamics on chain extension in the melt, which contrasts with the predominance of structural factors such as the entanglement density on chain extension in the solid state. Indeed, in the case of elongational flow experiments,[47] the strain hardening of branched PEs, which is relevant to chain extension, can be reduced to about nothing if the timescale of the experiments is comparable or greater than the relaxation time. This is a clear indication of the

transient character of the chain network in the melt, which may disentangle under extensional flow at a low strain rate. For linear PEs, no strain hardening of the elongational viscosity suggests a high capacity for chain disentanglement during extensional flow. In the solid state, chain extension is governed by the entanglement density, which determines the strain hardening.[48] The lower strain hardening of branched PEs may be ascribed to a low entanglement density.

The ability of polymer chains for intertwining in the melt is mainly connected to the chain flexibility, which is explained by the so-called C_∞ parameter. Besides this parameter, the overlapping capability of the chain coils of a given polymer species, such as PE in this instance, is highly sensitive to the molecular architecture of the chains. If we neglect thermal expansion effects, the degree of chain overlap in the melt can be defined as the ratio

$$X = \rho/\rho_{app} \quad (1)$$

of the actual density of molten PE, $\rho \approx 0.85$ g/cm^3, to the apparent density of the chain coils, ρ_{app}. Indeed, if we consider an isolated chain of molar weight M, the X parameter provides an estimation of the number of parent chains of the same molar weight that must intertwine within the volume embraced by the isolated chain in a random coil conformation to achieve the actual density of the molten polymer. The apparent density of the isolated chain can be estimated from the ratio of the molar weight to the volume of the sphere of radius equal to the radius of gyration of the random coil, R_g, because this sphere enfolds more than 90% of the segments of the chain coil.[49] For linear PE and ethylene copolymers, one may consider the following relationship established from literature data:[50]

$$R_g \approx 1.26M^{1/2} \quad (2)$$

where R_g is given in nanometers and M is given in kilodaltons. Now, if we consider a linear low-density polyethylene (LLDPE) chain with $M = 100$ kDa, that is, about the weight-average molecular weight (M_w) for the polymers investigated in this work, it turns out that R_g is approximately 12.6 nm, and the apparent density is $\rho_{app} \approx 0.02$ g/cm^3. Borrowing from Kuhn and Kromer's[32] study of the molecular architecture of HP-LDPE, we have sketched Figure 6 a chain of molar weight $M = 100$ kDa of the single-autoclave HP-LDPE in a branch-extended conformation. The HP-LDPE molecule notably exhibits 10 LCBs with an average molar weight between LCBs close to 6 kDa. One may estimate to about 42 kDa the molar weight of its main chain, which is shown as a bold line in Figure 6. Assuming, in the first approximation, that LCBs do not significantly change the chain conformation in the melt, one may estimate the radius of gyration of the HP-LDPE chain coil, $R_g \approx 8.0$ nm, from the length of its main chain with eq 2. The apparent density of the HP-LDPE chain coil is, therefore, $\rho_{app} \approx 0.08$ g/cm^3.

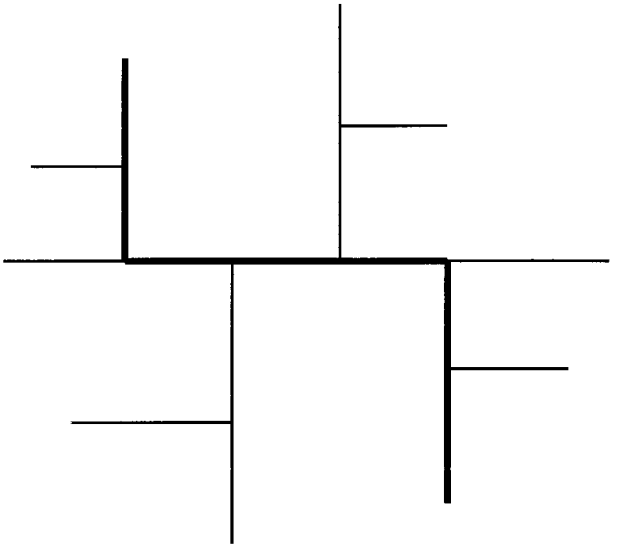

Figure 6. Schematic drawing for the molecular architecture of an HP-LDPE branched chain with a molar weight of 100 kDa.

Despite numerous assumptions, the aforementioned apparent density data reveal that the chains are deeply interpenetrated in the molten materials: for a chain of molar weight $M = 100$ kDa, the degree of chain overlap is $X \approx 50$ for LLDPE and $X \approx 12$ for HP-LDPE. Besides, these data show that chain overlap is much greater for LLDPE than for HP-LDPE.

This finding suggests that interchain entanglements, which provide the strength of the molecular network in the melt and in the solid state, are significantly more numerous in linear chains than in branched chains. Indeed, reduced overlapping reduces the probability of neighboring chains intertwining with each other. This has already been claimed to be an explanation for the

higher strain hardening of linear PEs in the solid state.[38] Of course, LCBs can make entanglements among themselves, within the sphere of gyration of the coil, but these intramolecular entanglements only contribute to the coil stiffness instead of the network strength. However, as previously pointed out, the strain hardening in the melt is lower for linear PEs than for branched PEs. This phenomenon, apparently contradicting the higher entanglement density of linear PEs, can be explained by dynamic effects during the extensional flow in the melt,[47,51] namely, a lower resistance to either disentanglement or strain-induced orientation of linear chains in comparison with branched chains. The longer relaxation time in the melt of branched PEs (see Table 1) supports this proposal of reduced chain dynamics due to LCBs.

Chain Unfolding versus Chain and/or Lamellar Orientation

Several authors have recently suggested that the orientation of lamellar stacks in blown films is responsible for unbalanced properties,[24,29–31] in contrast with most authors, who incriminate molecular orientation. Lu et al.[30,31] notably showed that processing conditions that promote randomly oriented lamellar stacks reduce mechanical anisotropy and improve dart impact resistance. Our data on M-LLDPE thoroughly support this finding. However, because ZN-LLDPE and HP-LDPE display the same type of texture, with the lamellae preferentially oriented normal to MD, the reverse trend of the two types of films with respect to MD and TD tear resistance reveal that the real situation is somewhat more complex than that previously described. We suggest that, beyond lamellar and chain orientations, chain unfolding is a factor of prime importance.

It is quite obvious that the unfolding of the chains during the blowing process increases the density of chain segments lying in the plane of the film. If one intuitively considers that tear resistance is governed by the frequency of such chain segments that oppose themselves to the propagation of the crack, one should expect an improvement of tear resistance with increasing chain extension. The drawability and shrinkage data from Table 1 clearly show that the ZN-LLDPE film has preferred chain extension along MD, and this means that more chain segments will bar the way to the crack propagation along TD in comparison with MD. This is why ZN-LLDPE has greater tear resistance in TD than in MD.

Regarding the HP-LDPE film, both drawability and shrinkage show that there is a high degree of chain extension along MD and moderate chain extension along TD, the latter being significantly higher than that for ZN-LLDPE and M-LLDPE. An explanation for this is that the branches of the star-shaped macromolecules are unfolded in the two main directions during the blowing process, and only a part of this unfolding can be relaxed before crystallization because of the rather high relaxation time. The chain extension that is frozen in the film is greater along MD because of the higher value of TUR with respect to BUR. In addition, because the chains are not ideally spherical but consist of a main chain with lateral LCBs, as sketched in Figure 6, this main chain is likely to preferentially unfold along MD during the blowing process because TUR $\gg$ BUR and also because of a suspected much longer relaxation time of the main chain in comparison with that of the LCBs. Consequently, the LCBs should act as molecular arms, slightly extended in TD, all along the main chain. If this is the case, a propagating crack would cross more chain segments in MD than in TD. This provides an explanation for the greater tear resistance of HP-LDPE in MD than in TD, that is, a reverse behavior of that of ZN-LLDPE. Nevertheless, the overall higher level of tear resistance of the latter can be explained by the higher degree of chain overlapping of ZN-LLDPE, which involves a higher degree of chain entanglement and, therefore, a higher mechanical strength of the macromolecular network.

The fact that the M-LLDPE film is challenged by the ZN-LLDPE film with respect to the level of the tear resistance in both MD and TD, despite its well-equilibrated tear behavior and better puncture resistance, deserves special attention. The explanation is straightforward in consideration of our previous argument on the density of chain segments that can act as obstacles to the propagation of the crack during the tear test. Indeed, the nearly isotropic M-LLDPE film necessarily contains fewer chain segments oriented parallel to the film plane than the ZN-LLDPE film to make opposition to either MD or TD tear. It is, therefore, suggested that isotropy is beneficial for puncture resistance because of the high drawability afforded by the chain in a random coil conformation, but this is not favorable for optimum tear resistance, despite good balance.

Finally, a last comment should be made regarding the shape of the stress–strain curve along MD of the HP-LDPE film, the yield stress being 50% higher than that along TD, as well as that of the isotropic material. This phenomenon has been reported previously for branched PEs[38] but never for linear PEs. This cannot be explained solely by the high degree of chain extension along MD. We suspect that the strong orientation of the crystalline lamellae with their normal along MD, as judged from SAXS [Fig. 1(a)], prevents the plastic shear processes through both the sample width and thickness of the film because the resolved shear stress (RSS) on the (hk0) slip planes is nil. Plasticity may only take place after some tilt of the lamellae to orient the slip planes toward the maximum RSS. Rotation about the b axis is by far the most easy tilt process because of the rather large form factor of the lamellae. However, the high degree of chain extension along MD, already discussed, is likely to hinder the lamellar tilting as the applied tensile stress increases. The critical RSS in the crystalline lamellae will then be reached after the applied tensile stress has jumped much above the value required for yielding for the corresponding isotropic sample.

Isotropy versus Orthotropy

ZN-LLDPE exhibits better tear resistance than M-LLDPE, despite its anisotropy. In contrast, isotropic M-LLDPE has a better puncture resistance because of high drawability with high energy absorption. Therefore, if the chain extension that takes place during blowing involves an increase in the chain segment density within the film plane that is beneficial for tear resistance, it is quite clear that isotropy is beneficial for puncture resistance. One may, nevertheless, wonder if orthotropy, involving equilibrated chain extension along MD and TD, would not be the best way for optimum puncture and tear resistance, with a fair balance of the latter along MD and TD.

Metallocene PEs have short relaxation times in the melt that make them able to recover most of the chain extension developed during the time of the blowing before crystallization. This is the reason for the fair isotropy of the films, which accounts for the mechanical properties. Linear PEs can also be blown into nearly isotropic films, but the reasons are quite different. TUR and BUR are generally the major factors of film texturing. The common situation, with TUR greater than BUR, leads to the row structure with the crystalline lamellae normal to MD. Reducing the TUR/BUR ratio provides a means of reducing the structural anisotropy and improving in parallel both the puncture resistance and tear resistance balance.[18,25,29–31] Unfortunately, this situation is too far from industrial conditions of film blowing. However, the deformation path of the molten material during tubular blowing is strongly dependant on the processing parameters, such as the stress, air velocity, and freeze-line height. Those parameters may be adjusted for re-equilibrating the difference of chain extension induced by the largely unbalanced TUR and BUR. The deformation path can notably be modified by changes in the freeze-line height.[28,30,31,52,53] Therefore, the shape of the bubble in the deformation zone between the die and the crystallization line may have the form of either a bowl or a stemmed glass,[52] depending on whether film stretching along MD and TD takes place in a simultaneous or sequential manner, respectively. This involves a modification of the molecular extension processes and notably enables a more important relaxation-induced rearrangement of the chains in the direction in which chain extension occurred first.[30,31,53] This was the way used by Lu et al.[31] to reverse the MD-to-TD tear resistance ratio for HDPE films for the same TUR/BUR ratio of approximately 8. Despite this high TUR/BUR ratio, the authors showed that increasing the time allowed for MD chain relaxation involved a higher level of TD chain extension in comparison with MD, as revealed by the MD and TD tensile drawing curves.[31] This resulted in an unusual greater tear resistance for linear PE in MD than in TD.

Some authors have claimed that isotropy is favorable for film use properties.[10,18,19] However, it seems that the so-called isotropy of the films, judged either from two-dimensional structural studies in the plane of the film or from the comparison of MD and TD mechanical properties, might be, in fact, an orthotropy. Only metallocene PEs really display isotropy, regardless of blowing conditions, because of relaxation times much shorter than those for conventional linear or branched LDPE at an equivalent melt-flow index (MFI).

CONCLUSIONS

The tear and puncture resistance of films largely depend on the processing-induced texture. M-

LLDPE has a very short relaxation time in the melt in comparison with the time that the material remains in the molten state between the die and the frost line. This enables the chains stretched by the blow-up and take-up to relax to a nearly isotropic state. This almost annihilates film texturing and imparts better dart impact performances in comparison with those of ZN-LLDPE and HP-LDPE. The slightly higher strain hardening of M-LLDPE, which is ascribed to a very small number of LCBs, also contributes to its high puncture resistance.

The better use properties of ZN-LLDPE in comparison with those of HP-LDPE are assigned to better chain intertwining and higher strain hardening in the solid state. The opposite behavior of the two materials with respect to the unbalanced tear resistance of the films is ascribed to the chain architecture: linear chains mainly unfold along MD for ZN-LLDPE, whereas chains with LCBs unfold along both MD and TD for HP-LDPE.

Even though M-LLDPE provides the best compromise of maximum puncture resistance and quite high and well-equilibrated tear resistance, it is not as good as ZN-LLDPE with respect to the tear resistance level. This is attributed to the nearly isotropic structure with an almost random chain distribution, which reduces the probability of chain segments lying within the film plane. These segments are the ones most prone to stop crack propagation. It is, therefore, suggested that orthotropy, with some degree of chain extension within the film plane, would be the better texture for optimized tear and puncture resistance for either ZN-LLDPE or M-LLDPE. HP-LDPE will never reach equivalent use properties because it lacks strain hardening.

The generalization of our conclusions to all kinds of PEs produced by similar polymerization methods cannot be made without precautions. However, a general conclusion is that the average relaxation time in the melt is a major factor for the development of texture and mechanical anisotropy. This may help us to understand some of the specific properties reported in the literature, notably in consideration of the time allowed to the various sequences of the blowing process. The knowledge of a whole distribution of relaxation times, in combination with a complete molecular characterization, would be a promising way to progress into the structure–property relationships of PE films.

REFERENCES AND NOTES

1. Gregory, B. H. Proceedings of the Specialty Plastics 94 Conference; Zurich, Switzerland, 1994; Maack Business Services: Zürich, Switzerland, 1994; Chapter 3, pp 1–12.
2. Batistini, A. Makromol Chem Macromol Symp 1995, 100, 137–142.
3. Knuuttila, H.; Lehtinen, A.; Salminen, H. In Metallocene based polymers: preparation, properties and technology; Schiers, J.; Kaminsky, W., Eds. Wiley: New York, 1999; Vol. 2, pp 365–378.
4. Maddams, W. F.; Preedy, J. J Appl Polym Sci 1978, 22, 2721–2738.
5. Maddams, W. F.; Preedy, J. J Appl Polym Sci 1978, 22, 2739–2750.
6. Maddams, W. F.; Preedy, J. J Appl Polym Sci 1978, 22, 2751–2763.
7. Choi, K.-J.; Spruiell, J. E.; White, J. L. J Polym Sci Polym Phys Ed 1982, 20, 27–47.
8. Han, C. D.; Kwack, T. H. J Appl Polym Sci 1983, 28, 3399–3418.
9. Kwack, T. H.; Han, C. D. J Appl Polym Sci 1983, 28, 3419–3433.
10. Sherman, E. S. Polym Eng Sci 1984, 24, 895–907.
11. Ashizawa, H.; Spruiell, J. E.; White, J. L. Polym Eng Sci 1984, 24, 1035–1042.
12. Schurzky, K. G. J Plast Film Sheeting 1985, 1, 143–151.
13. Gilbert, M.; Hemsley, D. A.; Patel, S. R. Br Polym J 1987, 19, 9–23.
14. Kwack, T. H.; Han, C. D.; Vickers, M. E. J Appl Polym Sci 1988, 35, 363–389.
15. Bibee, D. V.; Dohrer, K. K. Tappi Journal 1988, 71, 199–204.
16. Butler, T. I.; Patel, R. J Plast Film Sheeting 1993, 9, 181–200.
17. Butler, T. I.; Lai, S. Y.; Patel, R. J Plast Film Sheeting 1994, 10, 248–261.
18. Simpson, D. M.; Harrison, I. R. J Plast Film Sheeting 1994, 10, 302–325.
19. Patel, R. M.; Butler, T. I.; Walton, K. L.; Knight, G. W. Polym Eng Sci 1994, 34, 1506–1513.
20. Plumbey, T. A.; Sehanobish, K.; Patel, R. M.; Lai, S. Y.; Chum, S. P.; Knight, G. W. J Plast Film Sheeting 1995, 11, 269–278.
21. Fruitwala, H.; Shirodkar, P.; Nelson, P. J.; Schregenberger, S. D. J Plast Film Sheeting 1995, 11, 298–311.
22. Yu, T.-H.; Wilkes, G. L. Polymer 1996, 21, 4675–4687.
23. Kim, Y.-M.; Park, J.-K. J Appl Polym Sci 1996, 61, 2315–2324.
24. Kim, Y.-M.; Kim, C.-H.; Park, J.-K.; Lee, C.-W.; Min, T.-I. J Appl Polym Sci 1997, 63, 289–299.
25. Ghaneh-Fard, A. Proceedings of the International Symposium on Oriented Polymers—RETEC Con-

ference of the Society of Plastic Engineers, Boucherville, Canada, 1998; Industrial Materials Institute-Canada National Research Council: Boucheville, Quebec, 1998; pp 489–520.
26. Legros, N.; Cole, K. C.; Ajji, A. Proceedings of the International Symposium on Oriented Polymers—RETEC Conference of the Society of Plastic Engineers, Boucherville, Canada, 1998; Industrial Materials Institute-Canada National Research Council: Boucheville, Quebec, 1998; pp 129–138.
27. Kuijk, E. W.; Tas, P. P.; Neuteboom, P. J Reinf Plast Compos 1999, 18, 508–517.
28. André, J.-M.; Haudin, J.-M.; Labaig, J.-J.; Colin, J.-M.; Agassant, J.-F.; Demay, Y.; Monasse, B. Proceedings of the 14th Annual Technical Meeting of the Polymer Processing Society, Yokohama, Japan, June 1998; Polymer Processing Society: Akron, OH, 1998; pp 729–730.
29. Andre, J.-M.; Haudin, J.-M.; Labaig, J.-J.; Colin, J.-M.; Monasse, B. Proceedings of the 3rd Esaform Conference on Materials Forming, Stuttgart, Germany, April 2000; ESAFORM: Sophia Antipolis, France, 2000; pp V4–V7.
30. Lu, J.; Sue, H.-J.; Rieker, T. P. J Mater Sci 2000, 35, 5169–5178.
31. Lu, J.; Sue, H.-J.; Rieker, T. P. Polymer 2001, 42, 4635–4646.
32. Kuhn, R.; Krömer, H. Colloid Polym Sci 1982, 260, 1083–1092.
33. Vonk, C. G. In Small-Angle X-Ray Scattering; Glatter, O.; Kratky, O., Eds.; Academic: New York, 1982; Chapter 13.
34. Wunderlich, B. Macromolecular Physics; Academic: New York, 1971; Vol. 1, Chapter 4.
35. Usami, T.; Gotoh, Y.; Takayama, S. Macromolecules 1986, 19, 2722–2726.
36. Hosoda, S.; Uemura, A. Polym J 1992, 24, 939–949.
37. Flory, P. J. J Chem Phys 1949, 17, 223–240.
38. Hert, M.; Raviola, F. Plasticulture 1982, 54, 32–39.
39. Hunter, B. K.; Russel, K. E.; Scammell, M. V.; Thompson, S. L. J Polym Sci Polym Chem Ed 1984, 22, 1383–1392.
40. Gaucher-Miri, V.; Elkoun, S.; Seguela, R. Polym Eng Sci 1997, 37, 1672–1683.
41. Keller, A.; Machin, M. J. J Macromol Sci Phys 1967, 1, 41–91.
42. Keith, H. D. J Appl Phys 1964, 35, 3115–3126.
43. Nasagawa, T.; Matsumura, T.; Hoshino, S. J Appl Polym Sci Appl Polym Symp 1973, 20, 275–293.
44. Nasagawa, T.; Matsumura, T.; Hoshino, S. J Appl Polym Sci Appl Polym Symp 1973, 20, 295–313.
45. Ghaneh-Fard, A.; Carreau, P. J.; Lafleur, P. G. Proceedings of the 54th Annual Technical Conference of the Society of Plastic Engineers, Indianapolis, IN, 1996; Society of Plastic Engineers: Brookfield, CT, 1998; Vol. 1, pp 111–115.
46. Prasad, A.; Shroff, R.; Rane, S.; Beaucage, G. Polymer 2001, 42, 3103–3113.
47. Schlund, B.; Utracki, L. A. Polym Eng Sci 1987, 27, 380–386.
48. Seguela, R.; Rietsch, F. J Mater Sci 1988, 23, 415–421.
49. Tanford, D. Physical Chemistry of Macromolecule; Wiley: New York, 1961; Chapter 3.
50. Darras, O.; Seguela, R. Colloid Polym Sci 1995, 273, 753–765.
51. Leblans, P. J. R.; Bastiaansen, C. Macromolecules 1989, 22, 3312–3317.
52. Kanai, T.; White, J. L. Polym Eng Sci 1984, 24, 1185–1201.
53. Kanai, T.; Kimura, M.; Assano, J. J Plast Film Sheeting 1986, 2, 224–236.